Electronic Supplementary Material (ESI) for Materials Advances.

Sustainable Oxygen Evolution Catalysis - Electrochemical Generation of Mössbauerite *via* Corrosion Engineering of Steel

Sebastian Weiß,[a,b] A.V. Radha,[b] Michael Ertl,[b] Catherine McCammon [c] and Josef Breu [a,b*]

[a] Bavarian Center for Battery Technology (BayBatt), University of Bayreuth, Universitätsstr. 30, 95447 Bayreuth (Germany)

[b] Department of Chemistry, University of Bayreuth, Universitätsstr. 30, 95447 Bayreuth (Germany)

[c] Bayerisches Geoinstitut, University of Bayreuth, Universitätsstr. 30, 95447 Bayreuth (Germany)

* Correspondence to: josef.breu@uni-bayreuth.de

1. Cyclic voltammogram recorded during the deposition process

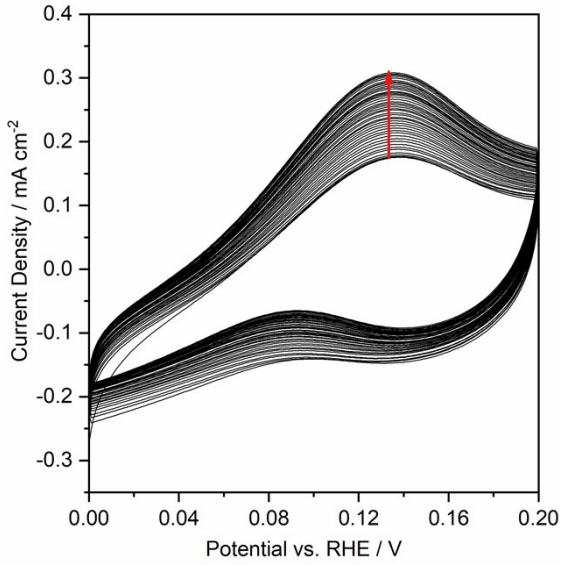

Fig. S1: Voltammogram recorded during the deposition of GR with a scan speed of 5 mV s^{-1}.

Cyclic voltammetry in the GR associated stability region was performed. The applied potentials ensure a suitable Fe^{2+}/Fe^{3+} ratio for the deposition of GR. Maximum anodic currents are found at 0.13 V vs. RHE. With increasing number of cycles, the current density increases from 0.175 mA cm^{-2} to 0.308 mA cm^{-2}.

2. Electrooxidation of Green Rust

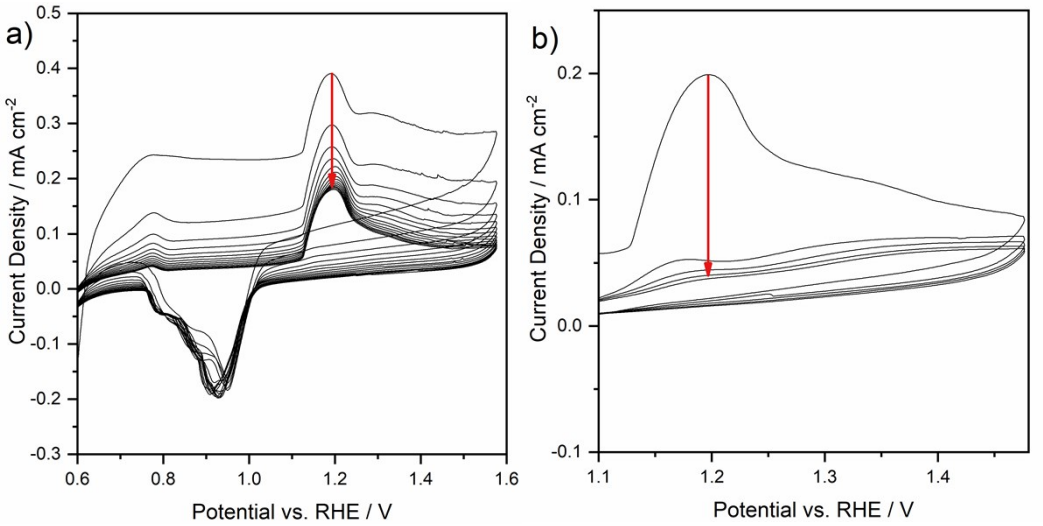

Fig. S2: a) Voltammogram recorded to identify a suitable oxidation potential to obtain GR* from GR. b) Voltammogram recorded during the oxidation of the material. Voltammograms were recorded with a scan speed of 5 mV s^{-1}.

Cyclic voltammetry was performed to identify a suitable oxidation potential to facilitate the oxidation of GR to GR*. For screening, a potential range from 0.6 V to 1.6 V was chosen. The recorded voltammogram features a small anodic wave at 0.78 V and an intense one at 1.20 V. A broad cathodic wave peaked between 0.95-0.91 V.

By reducing the potential range to 1.10-1.47 V, only the anodic event can be observed. Rapidly decreasing current densities indicate a quick oxidation process.

3. SEM micrographs of the oxidized and untreated samples

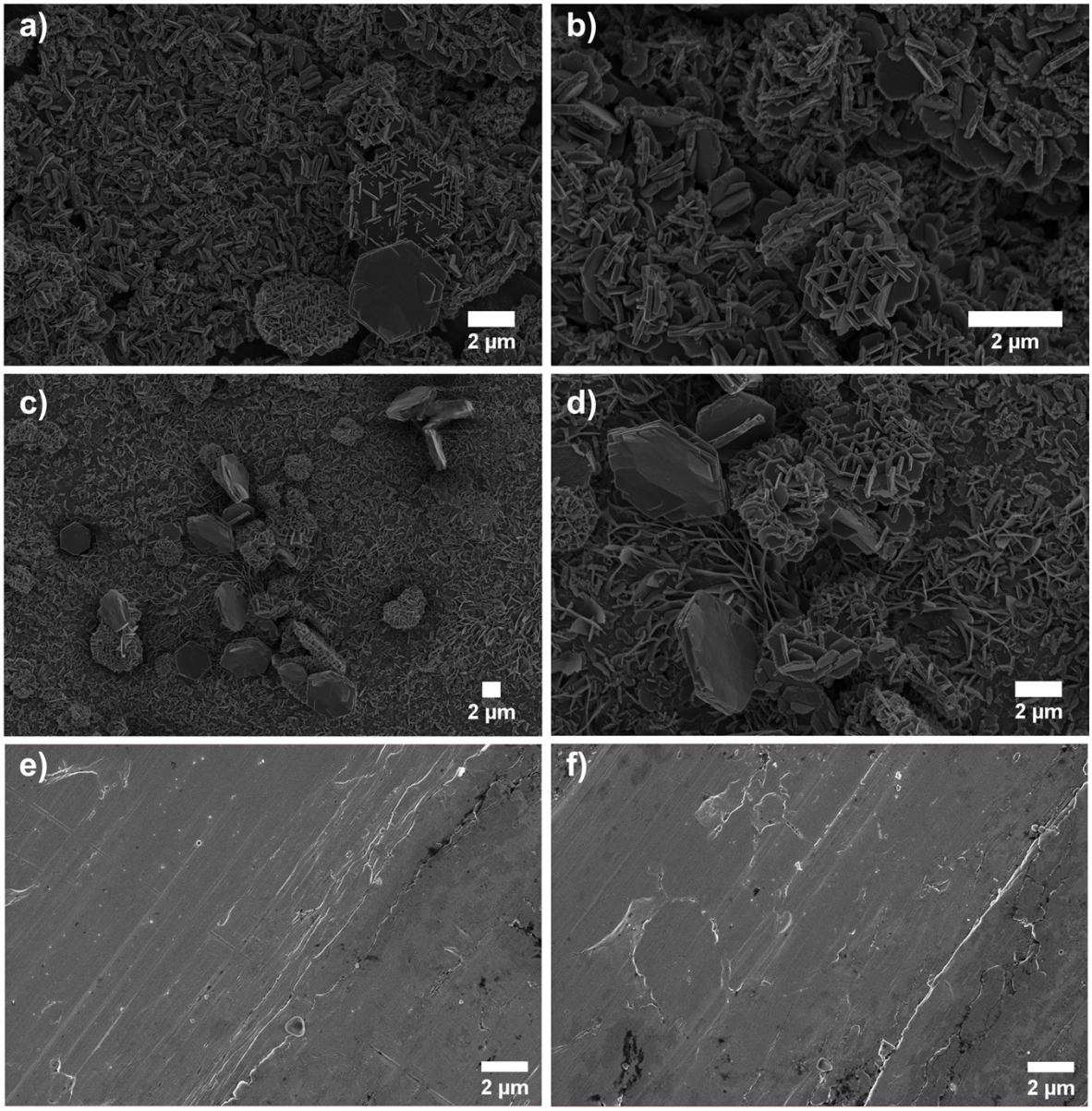

Fig. S3: SEM micrographs of the GR* samples. The GR^*_{ChOx} and GR^*_{ElOx} catalysts are shown in a,b) and c,d), respectively. Both feature similar morphologies of big, platy crystals intergrown with smaller platelets. In e) and f), the untreated steel plate is shown. Apparent roughness originates from the polishing procedure.

4. SEM micrograph of the unoxidized GR sample

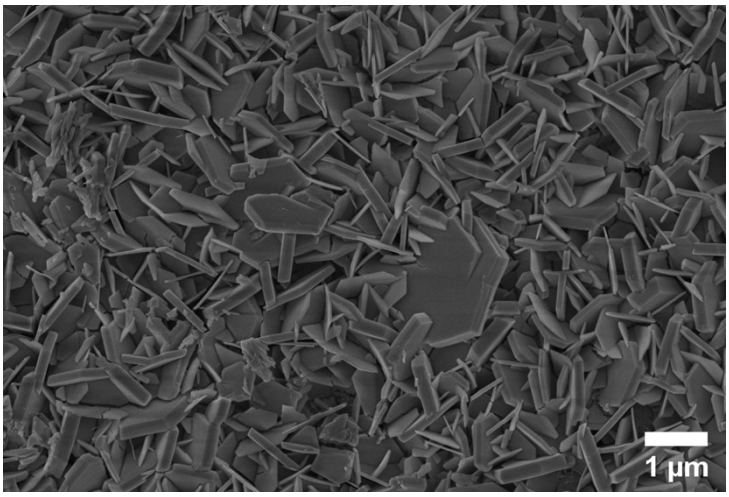

Fig. S4: SEM micrograph of GR before oxidation. The material features a similar morphology to these of GR*. Big, platy crystals intergrown with smaller platelets are observable and underline the assumption of a topotactic conversion from GR to GR^*_{ChOx} or GR^*_{ElOx}. Please note that partial oxidation is possible due to oxygen volatility and the necessary transfer of the sample.

5. Mössbauer spectroscopy

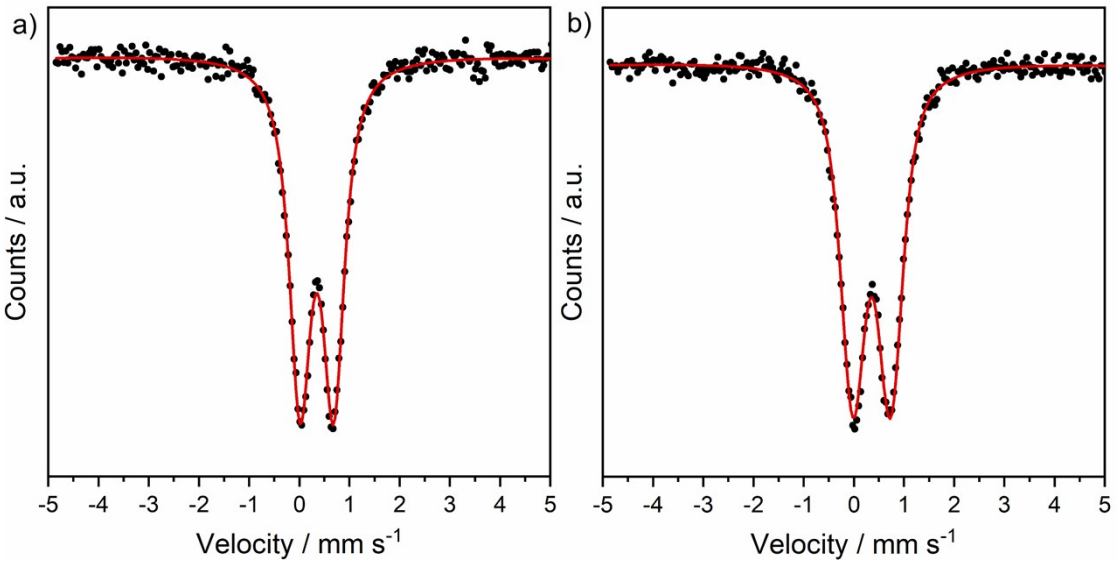

Fig. S5: Room temperature Mössbauer spectra of a) GR^*_{ChOx} and b) GR^*_{ElOx}. No Fe^{2+} impurities are detectable in either of the two samples.

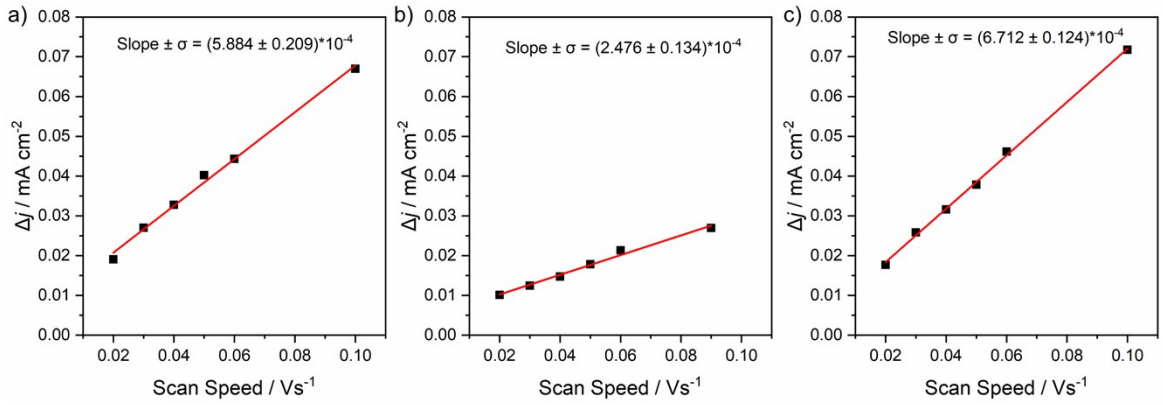

Fig. S6: Plots to determine the ECSA based on the difference between cathodic and anodic current depending on the scan speed: a) GR*$_{ChOx}$, b) blank substrate and c) GR*$_{ElOx}$.

6. Electrochemical Active Surface Area (ECSA)

7. ECSA normalized Linear Sweep Voltammograms

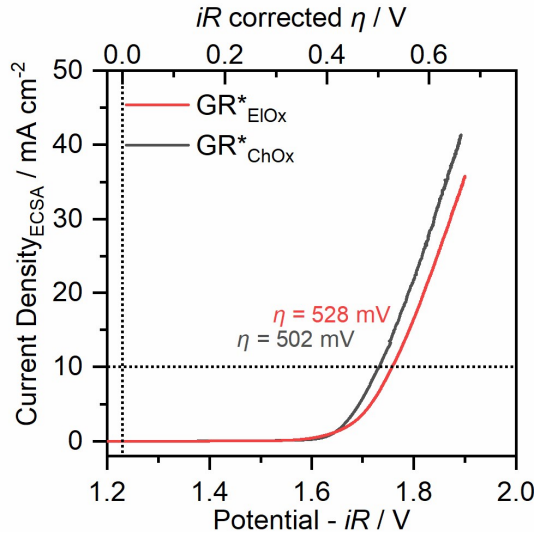

Fig. S7: ECSA normalized polarization curves of GR^*_{ChOx} and GR^*_{ElOx}. LSVs were recorded with a scan rate of 5 mV s^{-1} in O_2-saturated purified 1 M KOH solutions.

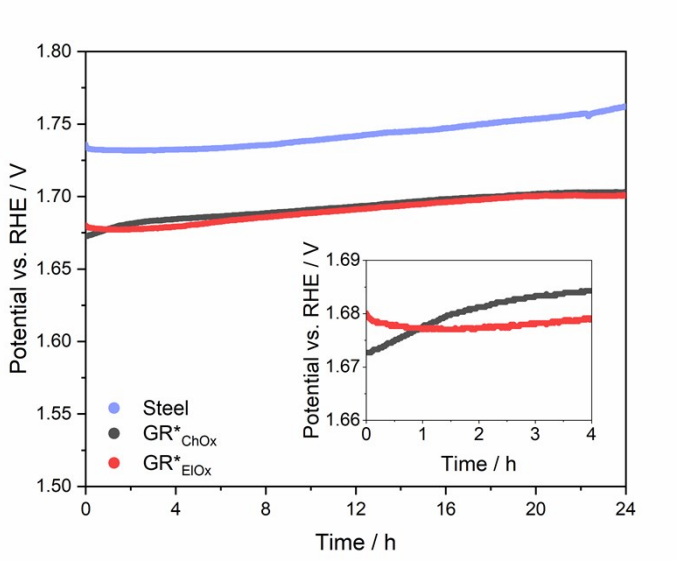

Fig. S8: Galvanostatic stability test of GR^*_{ChOx}, GR^*_{ElOx}, and steel in 1 M KOH at 10 mA cm^{-2} for 24 hours.

8. Galvanostatic stability tests

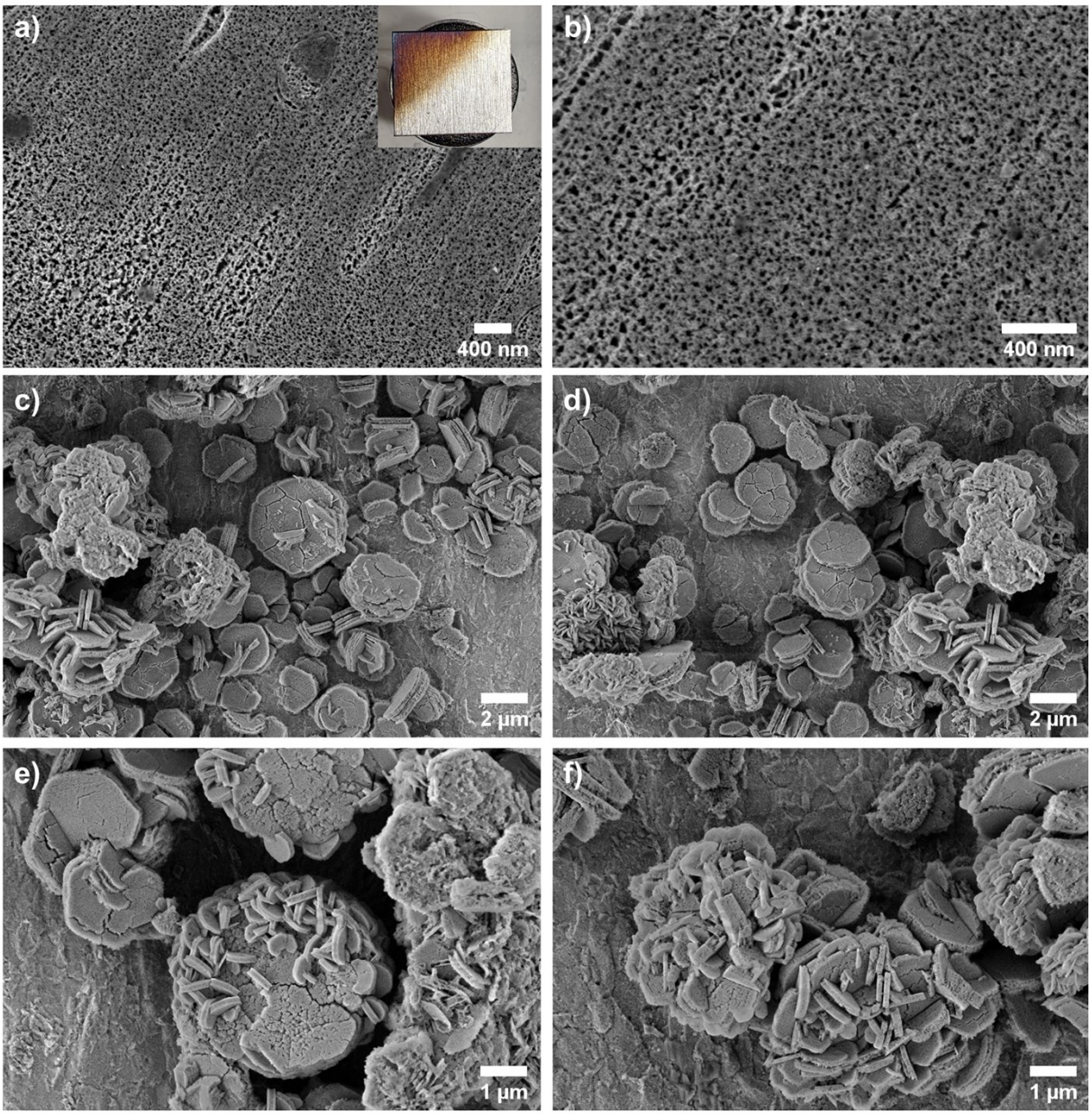

Fig. S9: Representative post-catalysis SEM micrographs for the bare steel (a,b), GR^*_{ChOx} (c, d), and GR^*_{ElOx} (e, f) sample after chronopotentiometry for 24 h at a current density of 10 mA cm^{-2}. Both samples show apparent degradation of the platelet-like catalyst morphology with some secondary deposit onto these platelets. A photograph of a partly immersed steel plate shows the apparent staining after electrocatalysis.

9. Post-catalysis investigations: Scanning Electron Microscopy

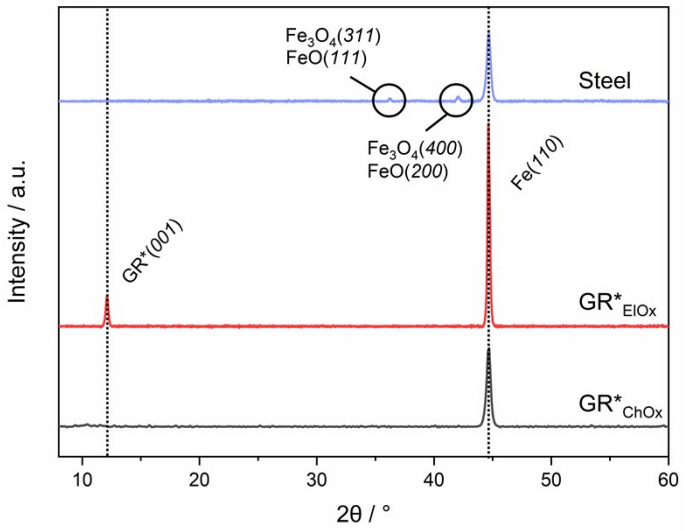

Fig. S10: Post-catalysis XRD patterns (Cu K_α source) of the bare steel substrate, the GR^*_{ChOx}, and GR^*_{ElOx} sample after chronopotentiometry for 24 h at a current density of 10 mA cm^{-2}. The bare steel substrate exhibits weak reflections which can be assigned to the presence of Fe_3O_4 (PDF #01-072-2303) and FeO (PDF #00-006-0615). GR^*_{ChOx} does not show any reflections, which indicates partial dissolution and thus the complete attenuation of the very weak (*001*) reflection. Due to the stronger initial intensity of the (*001*) reflection in GR^*_{ElOx}, the signal is still detectable post-catalysis.

10. Post-catalysis investigations: X-ray diffraction

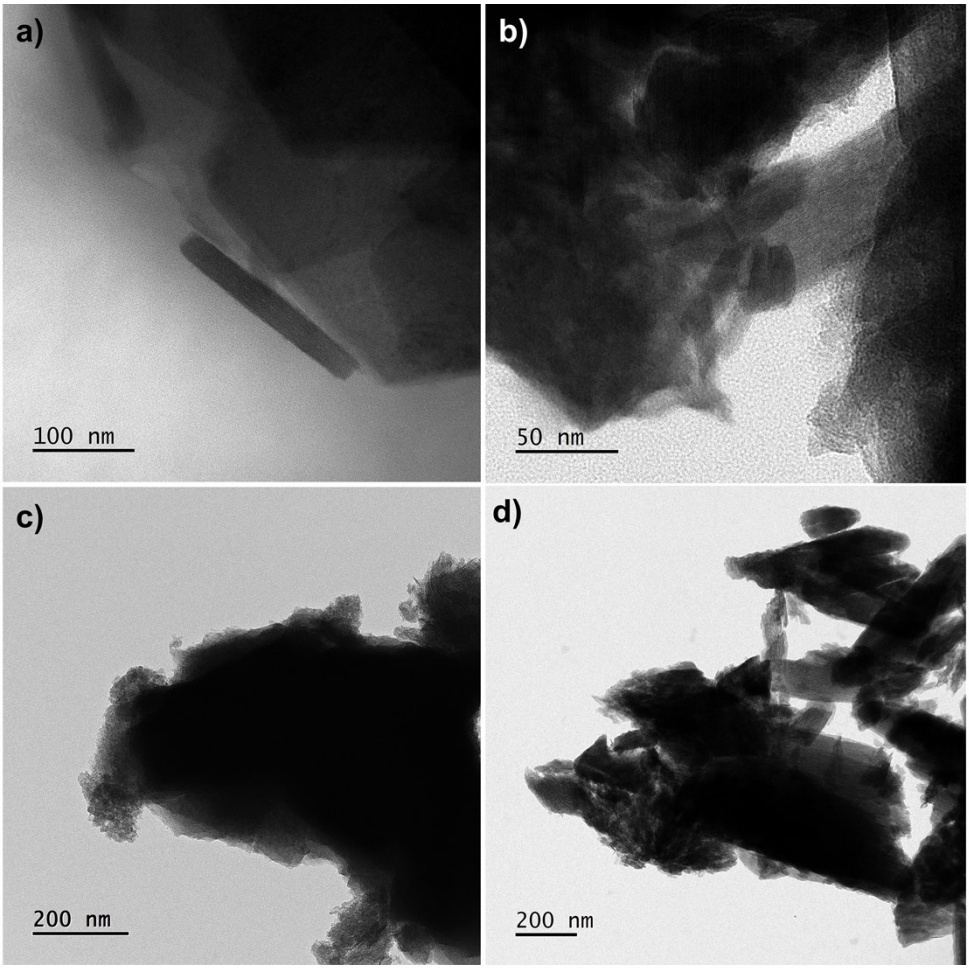

Fig. S11: Representative TEM micrographs from GR*$_{ChOx}$ (a), and GR*$_{ElOx}$ (b) before catalysis. Both feature similar morphologies of big, platy crystals partially intergrown with smaller platelets. The big platelets are composed of multiple individual layers. Post-catalysis TEM micrographs of GR*$_{ChOx}$ (c), and GR*$_{ElOx}$ (d) show that the platelet-like morphology is generally preserved but apparently overgrown by second phase.

11. Post-catalysis investigations: Transmission Electron Microscopy